

## Article

# New Insights into Fracture Porosity Estimations Using Machine Learning and Advanced Logging Tools

Ghoulem Ifrene \*, Doina Irofti, Ruichong Ni, Sven Egenhoff and Prasad Pothana 

Department of Petroleum Engineering, College of Engineering and Mines, University of North Dakota, Grand Forks, ND 58202, USA; doina.irofti@und.edu (D.I.); ruichong.ni@und.edu (R.N.); sven.egenhoff@und.edu (S.E.); prasad.pothana@und.edu (P.P.)

\* Correspondence: ghoulem.ifrene@und.edu

**Abstract:** Fracture porosity is crucial for storage and production efficiency in fractured tight reservoirs. Geophysical image logs using resistivity measurements have traditionally been used for fracture characterization. This study aims to develop a novel, hybrid machine-learning method to predict fracture porosity using conventional well logs in the Ahnet field, Algeria. Initially, we explored an Artificial Neural Network (ANN) model for regression analysis. To overcome the limitations of ANN, we proposed a hybrid model combining Support Vector Machine (SVM) classification and ANN regression, resulting in improved fracture porosity predictions. The models were tested against logging data by combining the Machine Learning approach with advanced logging tools recorded in two wells. In this context, we used electrical image logs and the dipole acoustic tool, which allowed us to identify 404 open fractures and 231 closed fractures and, consequently, to assess the fracture porosity. The results were then fed into two machine-learning algorithms. Pure Artificial Neural Networks and hybrid models were used to obtain comprehensive results, which were subsequently tested to check the accuracy of the models. The outputs obtained from the two methods demonstrate that the hybridized model has a lower Root Mean Square Error (RMSE) than pure ANN. The results of our approach strongly suggest that incorporating hybridized machine learning algorithms into fracture porosity estimations can contribute to the development of more trustworthy static reservoir models in simulation programs. Finally, the combination of Machine Learning (ML) and well log analysis made it possible to reliably estimate fracture porosity in the Ahnet field in Algeria, where, in many places, advanced logging data are absent or expensive.

**Keywords:** machine learning; SVM; ANN; fracture porosity prediction; anisotropy; well logging; shear waves; image logs



**Citation:** Ifrene, G.; Irofti, D.; Ni, R.; Egenhoff, S.; Pothana, P. New Insights into Fracture Porosity Estimations Using Machine Learning and Advanced Logging Tools. *Fuels* **2023**, *4*, 333–353. <https://doi.org/10.3390/fuels4030021>

Academic Editor: Manoj Khandelwal

Received: 31 May 2023

Revised: 26 July 2023

Accepted: 11 August 2023

Published: 29 August 2023



**Copyright:** © 2023 by the authors. Licensee MDPI, Basel, Switzerland. This article is an open access article distributed under the terms and conditions of the Creative Commons Attribution (CC BY) license (<https://creativecommons.org/licenses/by/4.0/>).

## 1. Introduction

Significant hydrocarbon resources may be derived from naturally fractured reservoirs such as fractured shale gas reservoirs, fractured tight sandstone and limestone reservoirs, and basement rocks [1–5]. Fracture characterization plays a critical role in the quantitative evaluation and effective management of these complex reservoirs [6]. Fracture characterizations include quantitative information on fracture density, orientation, and porosity, among others [7]. Fracture porosity directly controls the transportation and storage of hydrocarbons in these reservoirs. Additionally, the fracture properties affect the flow direction and permeability of the reservoir rocks [8]. Cores extracted during drilling, and less often, side wall cores, can be used to calculate fracture porosity [9,10]. However, this is an expensive and time-consuming process, and it can have a significant impact on the conclusions drawn if there are insufficient cores available for examination. On the other hand, empirical approaches, while easy to apply, are limited to wells from which data have been collected, resulting in a considerable level of uncertainty when combined with extrapolated or anticipated geological data [11]. To overcome these limitations, a cost-effective, rapid,

and reliable model is required for reservoir evaluations and characterizations to describe porosity, using well logs and existing core data to certify the results.

Artificial intelligence techniques are promising tools for addressing some of the complex problems in petroleum engineering, particularly when dealing with large datasets. In the oil and gas industry, machine learning uses computational algorithms and statistical models to analyze and interpret large volumes of data from various sources, such as downhole and surface sensors and equipment. It facilitates the identification of patterns, making predictions, and optimizing processes, thereby improving efficiency, reducing costs, and leading to better decision-making. Machine learning algorithms can be employed for reservoir characterization, production forecasting, anomaly detection, and predictive maintenance, among others. ML techniques are used in various applications for the exploration and production of hydrocarbons, for instance, in reservoir characterizations [12,13], production design [14], well completion [15], and drilling engineering [16]. A comprehensive review of the applications of artificial intelligence techniques in the context of petroleum engineering can be found in [17–20]. Researchers are investigating the application of machine learning techniques for fracture characterization. The authors of [21] characterized fractures using sonic waveform measurements and ML classification algorithms. The authors of [22] developed ML-based models to describe the fracture toughness in shales. The authors of [23] developed a technique called double beam neural network, which uses machine learning and was employed to convert double beam interference into a discrete fracture network; this technique is an image-to-image learning method. The authors of [24] carried out a computer vision-based structural analysis of a system containing granular and fracture porosity using K-means clustering algorithms. The primary emphasis of these investigations was on the characterization of various facets within a fractured reservoir, with the notable exception of fracture porosity. Furthermore, in instances where certain investigations have delved into ML applications to predict fracture porosity, they have predominantly relied on sophisticated image logs, core images [25], or production data [26], rather than on conventional well logs, which are more widely accessible.

Over the past decade, there has been a surge in research efforts aimed at predicting fracture porosity in geological formations using machine learning techniques. Researchers have explored various methodologies, from traditional regression models to more advanced artificial intelligence algorithms. Many studies have focused on integrating geological data on, for example, lithology, mineralogy, and seismic attributes with well log and core sample data to train predictive models. Moreover, the incorporation of unconventional data sources like image logs and microseismic data has shown promising results in enhancing the accuracy of predictions. Additionally, some studies have explored the application of neural networks, support vector machines, and random forests to tackle the complexity of fracture networks and their influence on porosity. Despite these advancements, challenges remain when handling sparse and noisy data, as well as in ensuring the interpretability of models and generalizing across diverse geological settings. Nevertheless, the literature reflects a growing consensus that machine learning has the potential to revolutionize fracture porosity predictions in reservoir characterizations and subsurface exploration. Table 1 summarizes some of the key literature in this field:

**Table 1.** Statistical characteristics for the used data.

Study	Methodology	Data Source	Key Findings
[27]	ANN	Caliper, Gamma Ray, Bulk Density, Neutron Porosity, Sonic Transient Time, and core data	ANN can be successfully used to predict the fracture density in boreholes using conventional well log data.
[28]	ANN	deep resistivity, density, neutron porosity and gamma ray	ANN has proven to be an excellent technique to estimate natural fracture porosity.
[29]	Bayesian Network Theory (BN) and Random Forest (RF)	Gamma-ray, deep resistivity, bulk density, neutron porosity, photo-electric.	BN Theory and RF were found to be effective in predicting the presence of fractures in different types of hydrocarbon-bearing rocks with a high degree of accuracy.
[30]	CNN (Convolutional Neural Network)	Seismic data, $V_p$ , $V_s$ , Image logs	The method offers a valuable means of evaluating fracture evolution in fractured reservoirs. Moreover, this research can serve as a benchmark for predicting anisotropic behavior and fracture porosity in other fractured reservoirs.
[31]	ANN	Image logs, gamma ray, caliper, photo-electric, deep resistivity, shallow resistivity	Interpreted FMI logs provide a trace while generating subsurface fracture maps using the statistical study of fracture radius, dip, and azimuth.

To the best of our knowledge, to date, very few studies have investigated the applicability of ML methods to predict fracture porosity derived from the integration of image logs and full acoustic waveforms. We employed two supervised learning methods, namely, Artificial Neural Network (ANN) and a hybrid method, ANN and Support Vector Machines, referred to as (SVM-ANN), and evaluated their efficacy in predicting fracture porosity. The novelty of the current research is its incorporation of hybrid machine learning algorithms into reservoir characterization. The importance of the present study lies in its leveraging of conventional logs to predict fracture porosity, making it possible to perform accurate reservoir evaluations and characterizations. This, in turn, facilitates enhanced decision-making and optimization of resources.

The input dataset includes the geophysical well logs of two wells in Ahnet, Algeria. These logs were taken through the Cambro-Ordovician formation and include caliper, compressional slowness, shear slowness, gamma ray, photoelectric factor, neutron porosity, and Bulk density logs. The ultimate objective is to develop a cost-effective and expeditious approach to predicting fracture porosity using well logs where core data are absent.

## 2. Geological Background

The Ahnet Basin is a Palaeozoic intracratonic sedimentary basin situated in the central and southern parts of the Algerian Sahara Massif [32] (Figure 1). It forms part of a series of north–south trending basins and basement highs, with the basin itself dipping toward the north. The Ahnet basin, situated in the northwest region of the Hoggar massif within the Algerian Sahara, is structurally unique due to its privileged location. It is bordered by the highly stable and rigid African Quest craton to the west, which has been cratonized for 3 billion years, and the mobile zones of the Hoggar craton to the east, which were cratonized during the Pan-African Orogeny (550 to 600 Ma). Furthermore, the basin is flanked by the highly stable Mole of In Ouzzal in the south. The suture zone between the Hoggar and African West Craton is marked by the folded NW–SE trending mountain chain of the Ougartha to the north. The unique structural setting of the Ahnet basin contributes to its geological diversity and has implications for hydrocarbon exploration and production in the area [33–36].

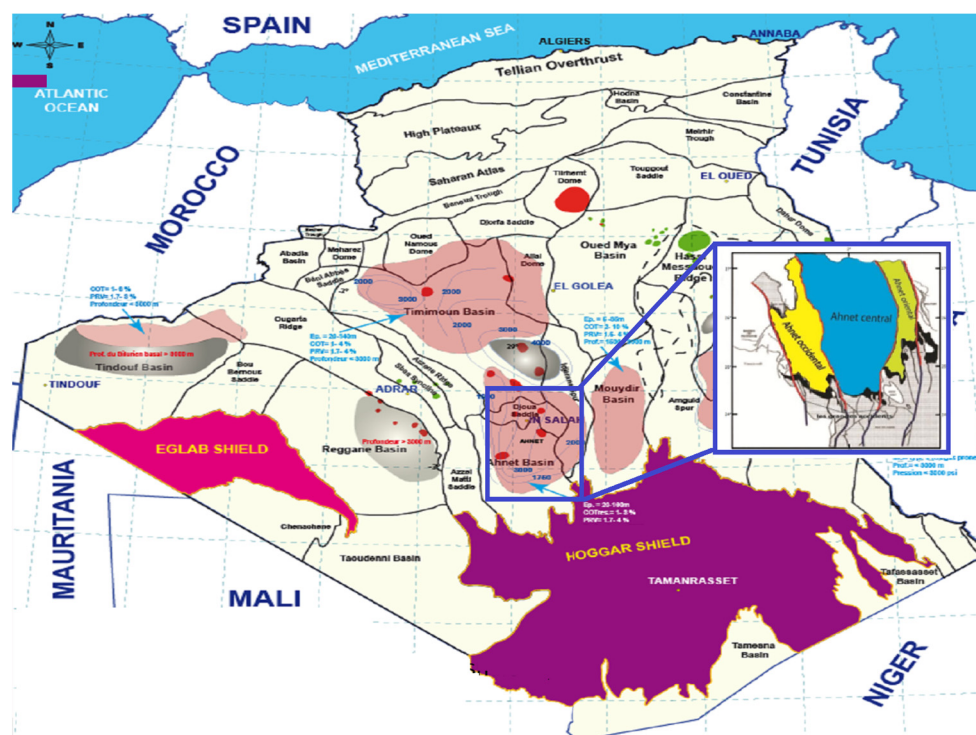
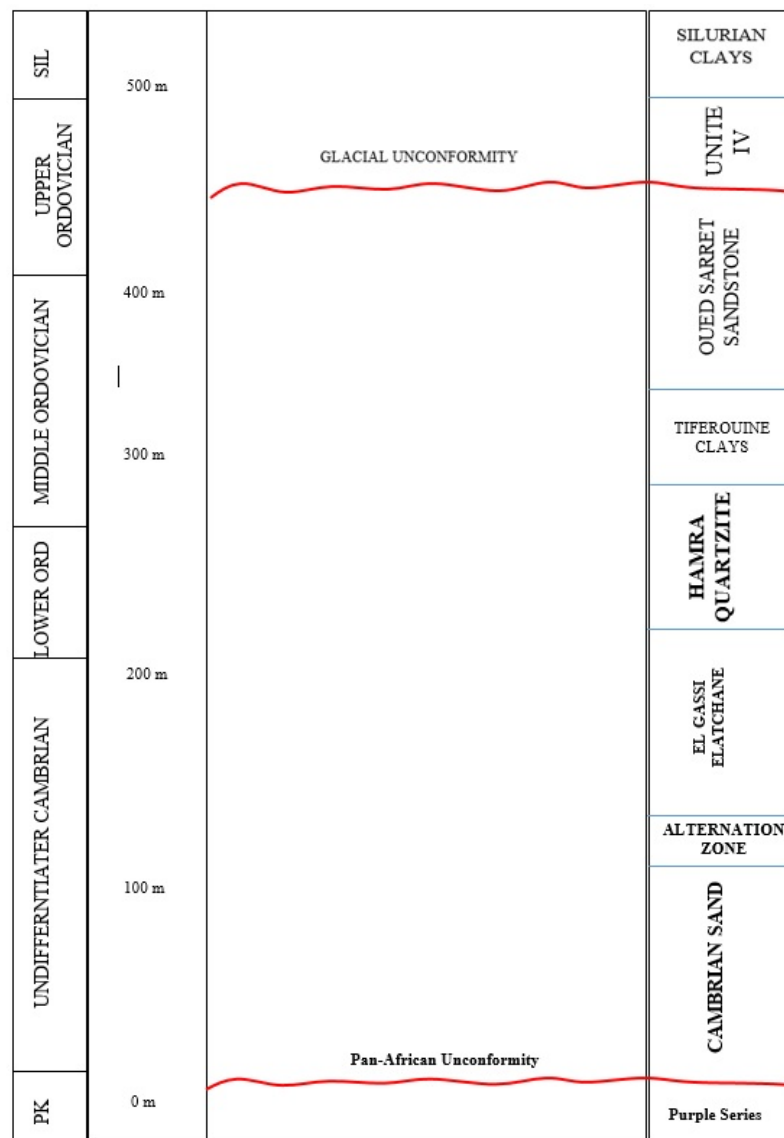


Figure 1. Location of the area of study.

The Paleozoic sediments of the Ahnet Basin overlie the basement rocks and are separated from them by an unconformity (Figure 2), which is typical of Saharan basins and grabens. The basement comprises thick series of little or non-metamorphosed Precambrian rocks, known as “Series Pourpres”, which exhibit substantially different mechanical properties from other basement rocks in the Sahara [34]. During the Cambro-Ordovician, a series of predominantly sandstones were deposited on the Precambrian basement [34]. These sandstones, which are more solid and cemented than those in other nearby basins, constitute the petroleum reserves in the South-Algerian basins. The natural fractures in the sandstones enhance the petrophysical characteristics of the reservoir. The Cambro-Ordovician series are typically divided into three sections. The lowermost section, Unit II, comprises mostly cross-stratified conglomeratic sandstones that were most likely formed in a fluvial environment. The overlying fine-grained and well-sorted sand and siltstones are interpreted as reflecting a marine influence; numerous *Skolithos* characterize these facies. Compared to the other Cambro-Ordovician reservoir units, this unit possesses good petrophysical properties, with porosity values that can reach 10% or more and permeability in the range of a few tens of mD. However, these reservoir characteristics are enhanced locally by natural fracturing. Unit III consists of alternating shales and sandstones and has a quartzite layer in the middle. This formation was deposited in a mixed continental to marine environment and is clearly transgressive at the scale of the Saharan platform. Locally, this formation rests unconformably on Unit II. Unit IV, the upper Cambro-Ordovician unit, is characterized by a marine and a glacial depositional environment. The facies of Unit IV correspond to medium to zero-quality reservoir characteristics in the Ahnet Basin.



**Figure 2.** Lithostratigraphic column of the Cambro-Ordovician formations in the Ahnet Basin, modified from [37].

### 3. Materials and Methods

#### 3.1. Fracture Porosity Quantification

The present study employed a workflow, as illustrated in Figure 3, for estimating fracture porosity. The methodology comprised an analysis of resistivity-based borehole images and the use of an acoustic scanning platform that integrated Shear Anisotropy and Flexural Dispersion Analysis (FDA). The process involved in generating borehole images from the initial observations of rock parameters included a series of procedures within the workflow. The input data were first subjected to depth shifting and speed correction during image log processing. Subsequently, pad and flap concatenation and equalization were employed during image generation to achieve clarity. To ensure accuracy, manual processing of the image logs and full acoustic waveforms was essential; this involved the precise picking of the fracture sinusoidal waves using Schlumberger’s Techlog software 2023.1.

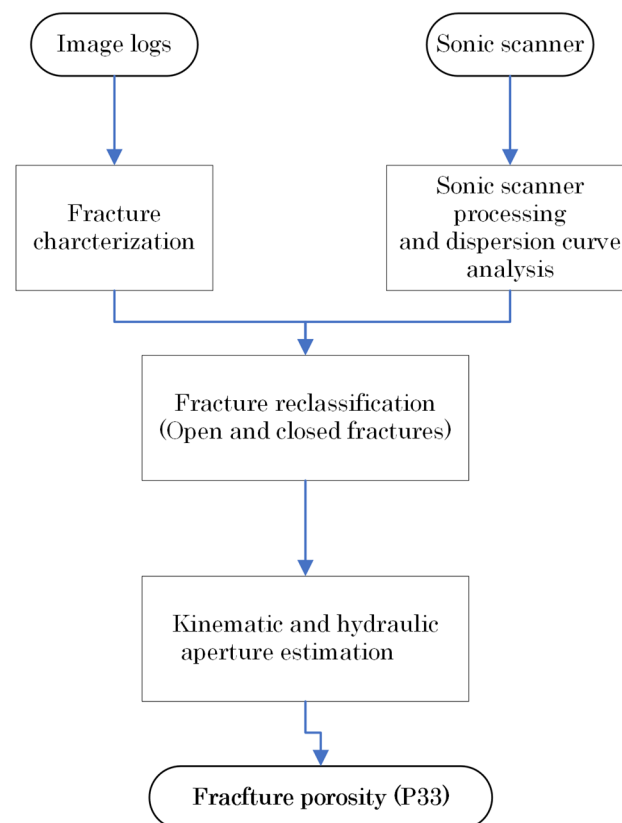


**Figure 3.** The proposed workflow for the fracture porosity estimation.

The process of estimating the fracture porosity involved the use of multiple techniques, as seen in Figure 4. The initial step involved analyzing the resistivity-based image logs, also known as FMI, to identify conductive fractures. However, it is important to note that these fractures may not necessarily be open, as they could be filled with minerals such as pyrite, chalcopyrite, or clays, all of which are electrically conductive.

To differentiate between the open and filled fractures, sonic scanner shear dispersion plots were employed to provide further insights into the nature of the fractures; this allowed us to identify 404 open fractures from a total of 635 fractures. Fractures present in rock formations can result in anisotropy, which is directional variation in the elastic properties of the rock. Acoustic anisotropy is responsible for the differing velocities of shear waves in various directions through the rock. Dipole flexural waves, being dispersive in nature, are influenced by several factors, such as borehole conditions, mud density and velocity, the logging tool used, and the formation properties. The sonic waveform dispersion analysis technique can be employed to study and describe the formation. This technique involves four possible mechanisms, one of which is inhomogeneous anisotropic, which is associated with fractures. In this mechanism, the shear wave separates into two components, with fast and slow frequencies falling within distinct ranges [38].

This workflow utilizes flexural wave shear anisotropy to determine the presence of fractures and distinguish between open ones and those filled with conductive minerals. A more accurate estimate of the fracture porosity can be obtained by combining the information obtained from the image logs and the sonic scanner shear dispersion plots.

To estimate the fracture porosity, it is essential to calculate the width of the fractures. Therefore, the aperture is calculated using Luthi and Souaite's (1990) equation:

$$w = cAR_m^b R_{xo}^{1-b}$$

$w$  = Fracture Width in mm

$R_m$  = Mud Resistivity

$R_{x0}$  = Formation Resistivity of the invaded zone  
 $A$  = Additional current into the formation  
 $c$  and  $b$  are tool parameters

Several factors impact the observed fracture aperture, including the resistivity of the drilling mud ( $R_m$ ) and invaded zone ( $R_{x0}$ ). To estimate the apertures, image logs are processed using advanced techniques that rely on measurements of excess current injected into the formation [39]. These images are calibrated using a shallow resistivity log.

The fracture volume is calculated using a simple volumetric formula that takes into account the fracture dip, borehole diameter, and estimated fracture width (kinematic aperture). The fracture porosity (P33) is then obtained by dividing the fracture volume by the borehole volume (Figure 5).

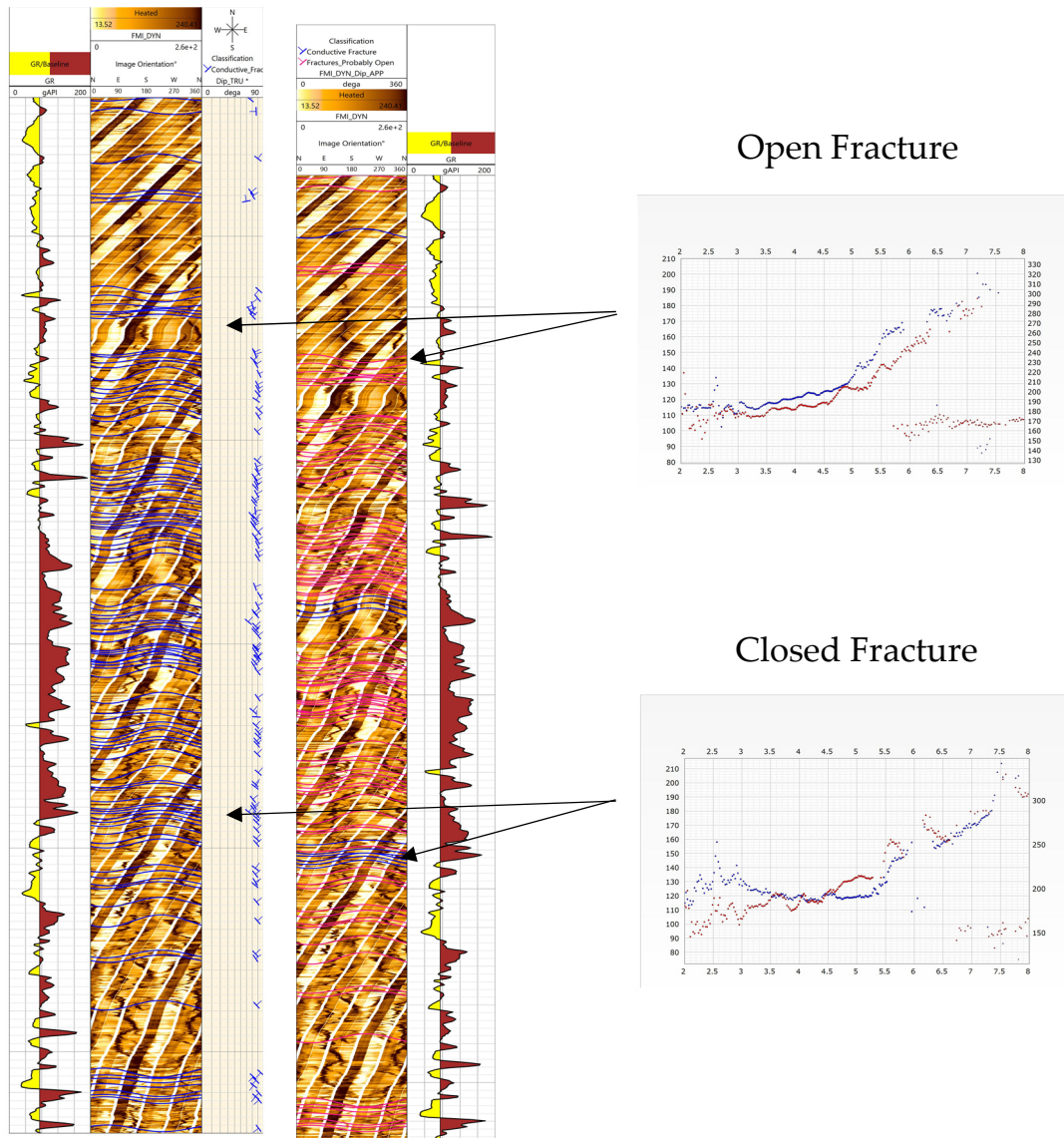
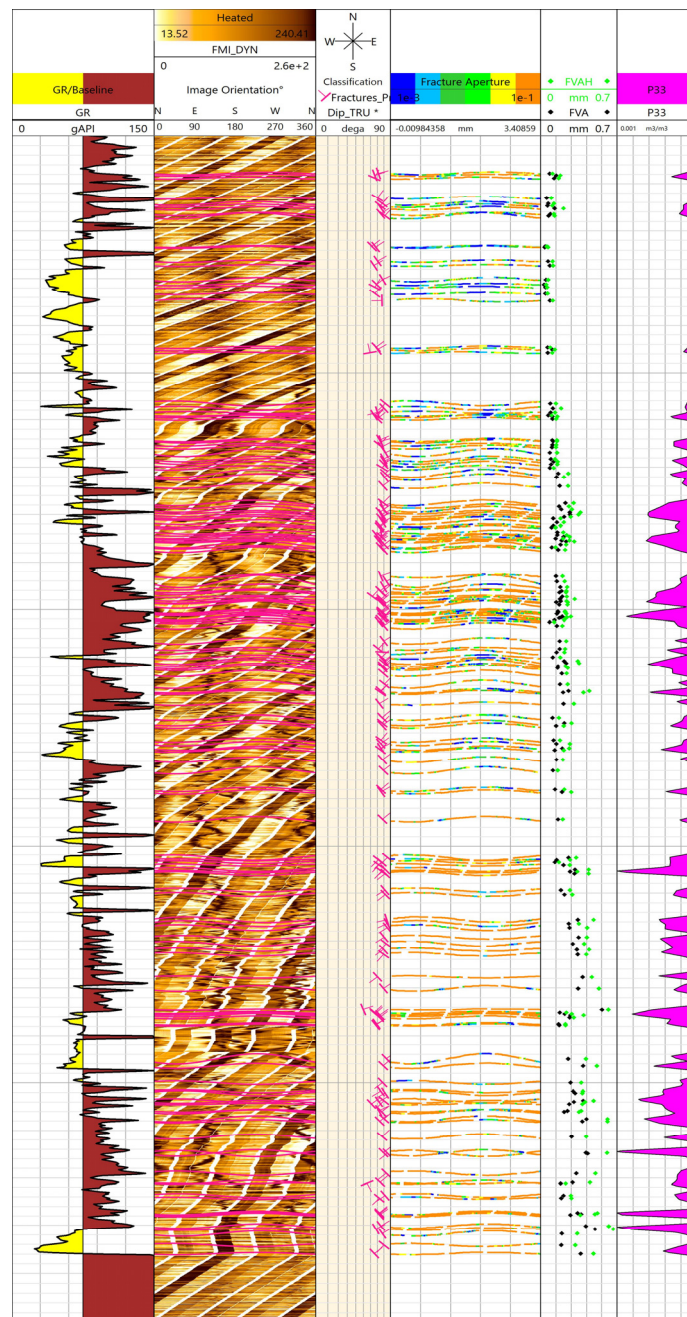


Figure 4. Fracture reclassification process using dispersion analysis plots.



**Figure 5.** Various rock characteristics as displayed in a typical borehole in the Cambro-Ordovician formation. Track 1: Gamma Ray (G.R.); Track 2: Dynamic Image log (FMI\_DYN) with open fracture lines; Track 3: Fracture tadpoles (dip and azimuth); Track 4: Fracture aperture along the fracture sine wave; and Track 5: Mean fracture kinematic (FVA) and hydraulic aperture.

### 3.2. Predictive Modeling Approach

#### 3.2.1. Exploratory Data Analysis

A combination of logs, i.e., depth, neutron porosity (Por), shear slowness (DTSM), compressional slowness (DTCO), natural gamma ray (G.R.), Bulk density (RHOZ), Photo Electric Factor (PEFZ), and caliper (Cal), was chosen in the present study to predict the porosity. The data consist of 5008 data samples and eight input well log attributes. Table 2 presents the data range for each of the input attributes used in this study, while Figure 6 illustrates the input logs used in the model. This step plays a critical role in comprehending our data by enabling us to visualize the distribution of each individual variable, as well as

the correlation among various features. Using pair plots, also called scatter plot matrices, is an effective tool for data visualization in research analysis. They allow us to look into the relationships among attributes within a dataset. The pair plot is a map of scatter plots where each variable in the dataset has been plotted against all other variables. The multivariate distribution can be obtained using a pair plot in R. Our analysis of the pair plot is provided in Section 4.

**Table 2.** Statistical characteristics for the used data.

	DEPT	Cal	DTCO	DTSM	GR	P33	PEFZ	Por	RHOZ
	(m)	(in)	(us/ft)	(us/ft)	(GAPI)	(v/v)	(b/e)	(v/v)	(g/cc)
count	5008	5008	5008	5008	5008	5008	5008	5008	5008
mean	2098.965	7.150779	64.1306	104.8334	118.4989	$7.74 \times 10^{-5}$	2.788434	0.040624	2.605229
std	165.4286	1.339378	5.422916	13.9901	70.87042	0.00016	0.815019	0.035257	0.080526
min	1793.596	4.243306	46.75045	79.24234	19.42065	0	1.781257	-0.01271	1.6979
max	2419.655	10.36588	88.15414	162.6788	734.3147	0.001278	10	0.37467	2.842013

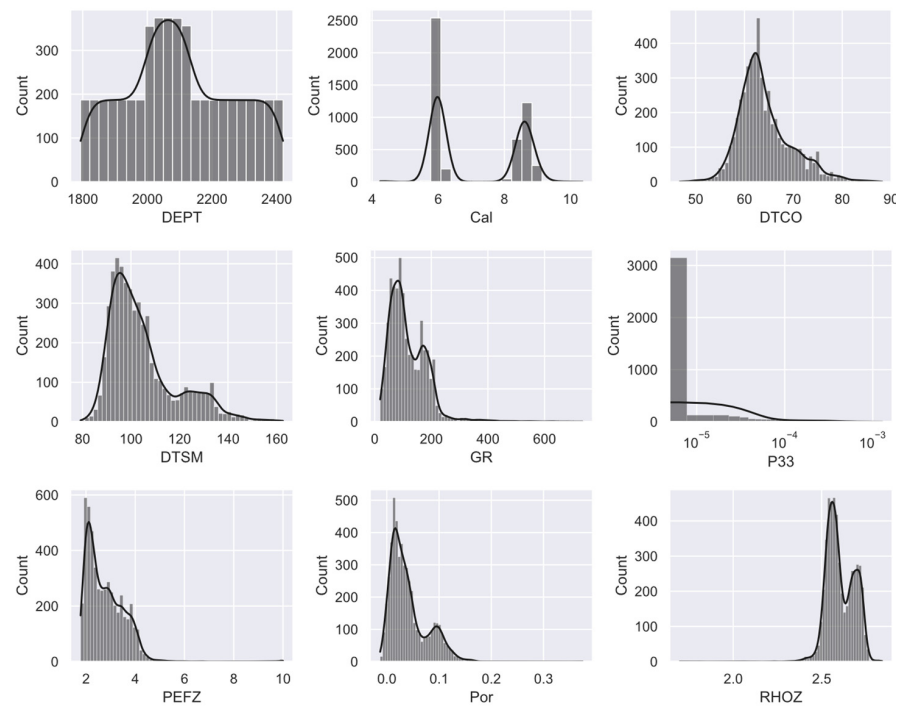


**Figure 6.** Data distribution of each input log and the P33. The corresponding statistical information and the units of each variable are provided in the Table 2.

Inaccurate data acquisition may occur due to various factors, including environmental conditions and inadequate instrument calibration. Therefore, the noise is eliminated by deleting any spiky readings and readings in front of washouts as shown in Figure 7.

### 3.2.2. Machine Learning Algorithms

Machine learning (ML) algorithms, which are a part of statistical methods, can be divided into four main types: supervised learning, unsupervised learning, semi-supervised learning, and reinforcement learning [40]. This paper focuses on the utilization of supervised ML methods to characterize the fractures, more specifically, fracture porosity. A supervised ML model learns from the training data that is assumed to be independent and identically distributed. The algorithm then uses an evaluation criterion to select the best model from a set of hypothesis spaces, which can make the best prediction under the evaluation criterion from training and test data [40].

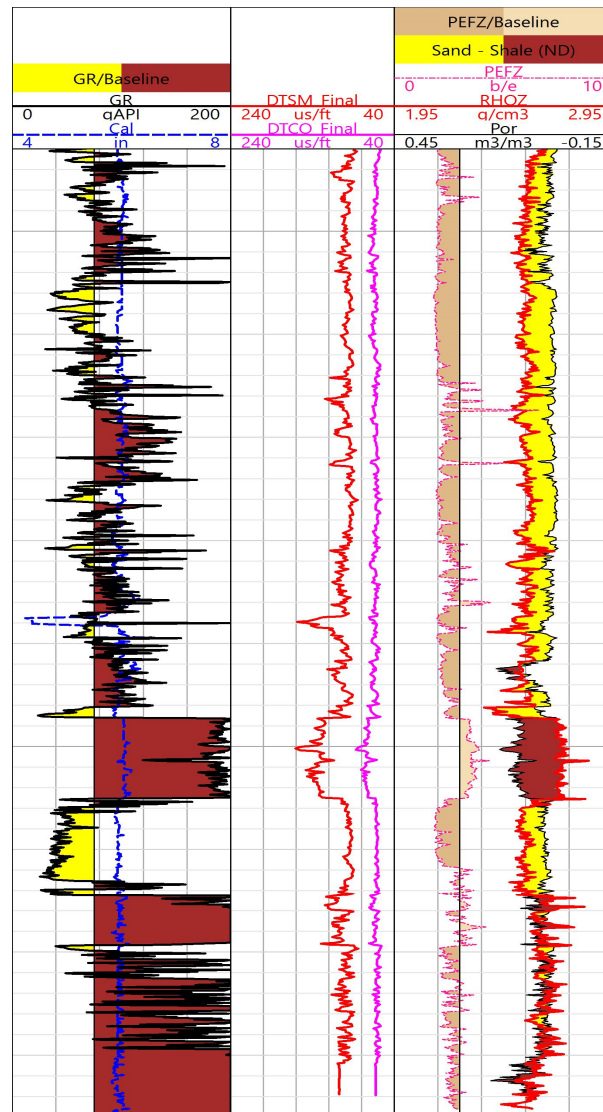


**Figure 7.** Input logs used for the fracture porosity prediction (Well B), Track 1: Gamma-ray (G.R.) and caliper (Cal) in yellow-brown and black; Track 2: Shear (DTSM) and compressional (DTCO) slowness in red and violet; and Track 3: Photo Electric Factor (PEF), Bulk density (RHOZ), and Neutron porosity (Por) in violet red, and black respectively.

We employed two machine learning methods in this study to predict the fracture porosity of the fractured reservoirs: (1) Artificial Neural Networks (ANN), and (2) Support Vector Machines + Artificial Neural Networks (SVM-ANN).

#### Artificial Neural Networks (ANN)

Artificial neural networks (ANNs) have become a powerful statistical tool in identifying and categorizing intricate outlines and systems beyond human intelligence [41]. As a type of supervised learning method, ANN models have three layers [42]: an input layer, a hidden layer, and an output layer. Further, the hidden layers can consist of one or more layers. During the calculation process, each node in the hidden layer will receive an input signal from its previous layer, which comprises all the nodes in that layer, along with their weighting factors [43]. The activation function, which could take different forms in each node, is used to tune the weighting factors of the nodes during the training process. The backpropagation algorithm minimizes the user-defined error metric between the model and the data [43]. Empirical studies have shown that ANN models can be effective in

estimating shear velocity and have the best regression performance results compared to other ML methods [44,45].

The initial approach involves utilizing the pure ANN model, which comprises two hidden layers and 7, 2 nodes, to forecast the fracture porosity (P33) in each layer, as illustrated in Figure 8. To accomplish this, the dataset is randomly split into two distinct parts, with the training data comprising 80% of the dataset and the test data 20%. The training data are utilized to train the ANN model, and the accuracy of the model is evaluated based on the metrics testing it on the test data. The objective function we used to train the data and validation was the Root Mean Squared Error (RMSE). This approach offers the advantage of balancing the contribution of errors from the entire range of fracture porosity values.

$$RMSE = \sqrt{\frac{1}{n} \sum_{i=1}^n (P_{33}^{Predicted} - P_{33}^{True})^2}$$

where  $n$  is the total number of observations,  $P_{33}^{True}$  are the actual data, and  $P_{33}^{Predicted}$  are the data predicted using a machine learning algorithm. This approach was implemented to assess the performance of the ANN model and to determine its suitability for the forecasting of P33.

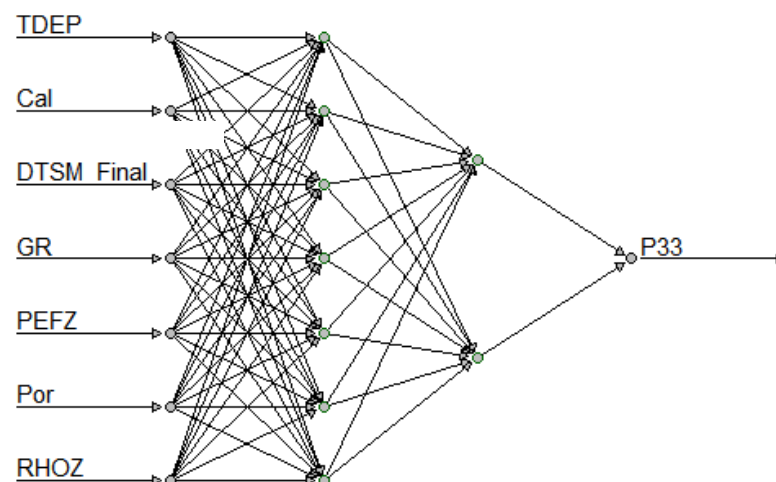


Figure 8. ANN Model architecture.

#### Hybrid Model Support Vector Machine-Artificial Neural Network (SVM-ANN)

A support vector machine (SVM) is a type of supervised learning method that can separate data into two classes [46]. Its basic model is a linear classifier that defines a decision boundary with the largest spacing in the feature space [46]. The SVM differs from other linear classifiers in that it maximizes the spacing or margin between the decision boundary and the closest data points. By using kernel tricks, SVM can also classify nonlinear data by transforming it into a higher-dimensional space where a linear boundary may be found. The learning strategy of SVM involves solving a convex quadratic programming problem to maximize the margin. Overall, SVM is considered the optimal algorithm for solving convex quadratic programming problems in supervised learning tasks [2].

The second approach employed in this project utilizes both SVM and ANN algorithms. The SVM algorithm determines the presence of fractures in formations by classifying the P33 variable into two categories: values of zero and greater than zero. An observed P33 value of zero indicates an unfractured portion of the formation, while a value greater than zero indicates the presence of fractures. Similar to the previous method, the dataset is randomly partitioned into two groups, namely, the training data and the test data. The SVM model is initially trained using the training data to distinguish between P33 values of zero and non-zero. At the same time, all datasets with a P33 value of zero are excluded from the training data. Subsequently, the ANN model is trained exclusively using data

from fractured formations. Finally, the accuracy of both models is evaluated using the test data (Figure 9).

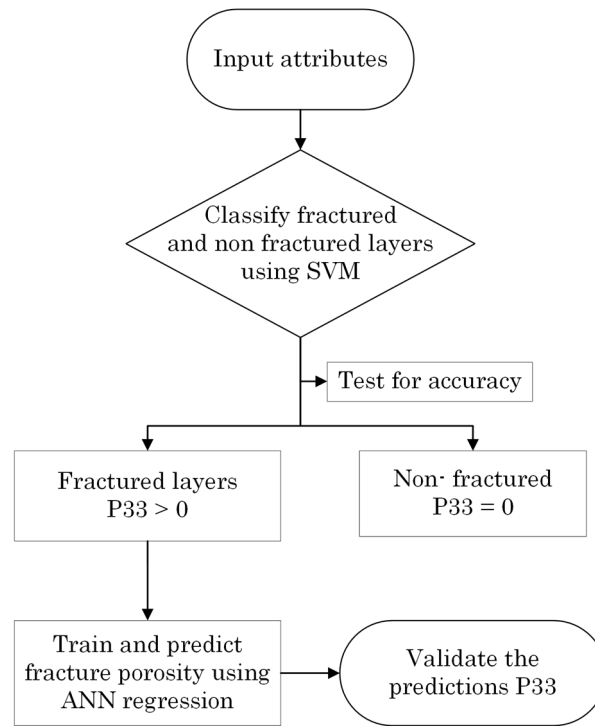


Figure 9. Flowchart for the hybrid model.

The ANN model used for the second approach (hybrid) has an architecture of two hidden layers and 10, 10 nodes on each layer, as shown in Figure 10.

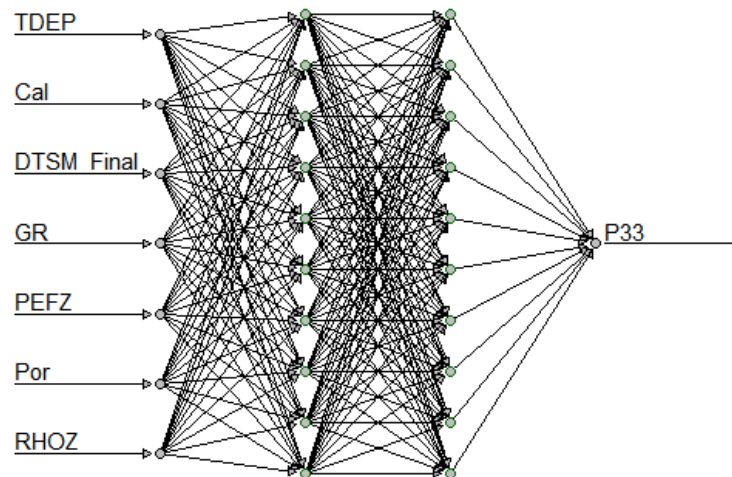
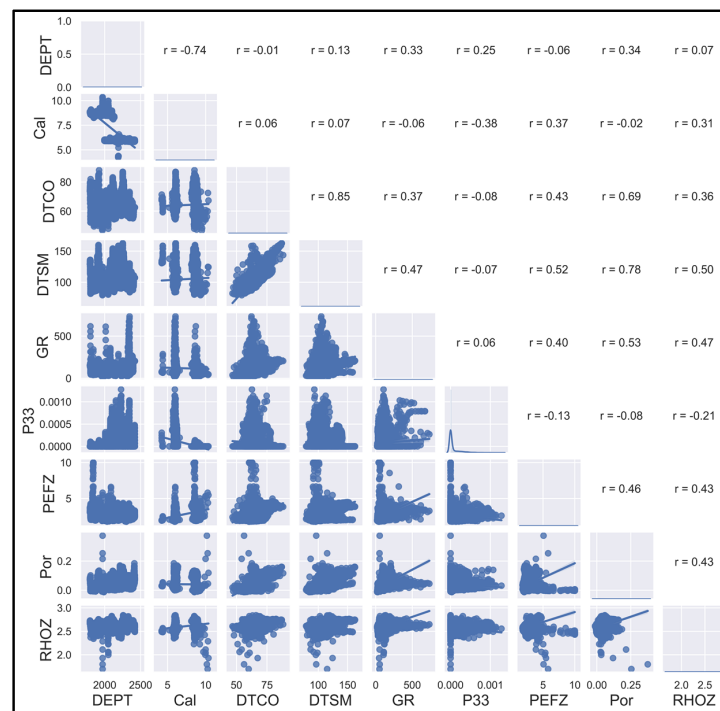


Figure 10. ANN model used for the hybrid approach.

#### 4. Results and Discussion

The pair plots were generated using R and are presented in Figure 11. The correlation plot indicates that the “DTCO\_Final” exhibited the weakest correlation with the P33, which represents the porosity of fractures. However, a nearly linear relationship was observed between the “DTCO” and the “DTSM”. Thus, when training the ANN and SVM-ANN models, the factor “DTCO” was removed from the model training. It can also be observed that P33 had a good correlation with the Bulk density (RHOZ) and photoelectric factor (PEFZ).



**Figure 11.** Pair plots of the input attributes and P33 data.

As mentioned earlier, the data consisted of 5008 samples which were randomly allocated into two groups. The first set contained 80% of the total samples, referred to as the “training data subset” and used to train the machine learning algorithms. The remaining 20%, known as the ‘test data subset’, were utilized to evaluate the efficacy of the machine learning methods. The error metric Root Mean Square Error (RMSE) was chosen to quantify the efficiency of the models.

Accurate estimations of fracture porosity are essential, as they play a vital role in assessments of hydrocarbon reserves. Machine learning (ML) algorithms have been increasingly employed in fracture porosity estimations due to their ability to handle large volumes of data and identify complex patterns. In this regard, two ML algorithms, i.e., pure Artificial Neural Networks and the hybrid SVM-ANN model, have been evaluated in terms of their effectiveness in estimating fracture porosity. This study aimed to provide insights into the comparative performance of these two ML algorithms and highlight the potential of hybridized machine learning algorithms in fracture porosity estimations.

#### 4.1. Artificial Neural Network (ANN)

We systematically investigated the optimum number of hidden layers and neurons in each layer required for the ANN model. Further, we observed the response of the objective function to determine the best network structure for our implementation of the neural network approach. We observed that increasing the number of layers and neurons increased the score of the objective function, although this was because of overfitting. Overfitting happens when a model is too complex and goes beyond the task of accurately fitting the patterns in the data, leading to it memorizing the training points. This causes the model’s performance to improve continuously on the training dataset; however, this improvement comes at the cost of the model’s ability to generalize to new, unseen data [47]. Due to noise in the training data and the potential inability to fully represent the entire population, it is crucial to prevent overfitting by carefully selecting the appropriate size for the neural network. The optimum ANN model consisted of two layers with 7 and 2 neurons in each layer. The ANN was implemented on R with algorithm backpropagation, weight backtracking, and the highest learning rate of 0.01.

The P33 predictions of the ANN are presented in Figure 12 the validity of the ANN was checked on separate data that were not used during training. We used RMSE to measure the performance and validity of the machine learning methods. We found RMSE values of  $4.13 \times 10^{-5}$  and  $20 \times 10^{-5}$  for Well A and Well B, respectively, as shown in Figure 12.

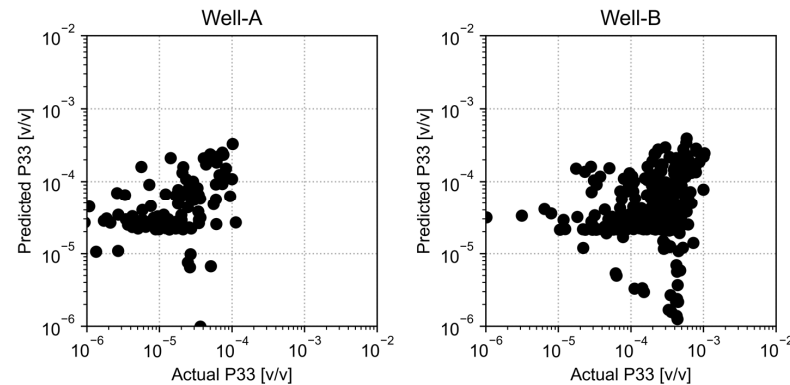


**Figure 12.** Cross plots of predicted data and the actual data used in the ANN model cross-validation.

The present study showcases the results obtained from our analysis, where we employed an Artificial Neural Network (ANN) to predict fracture porosity based on the provided input logs. The predicted values, alongside the corresponding input logs, are depicted in Figures A1 and A2. Upon examination, it became evident that the ANN predictions exhibited a discernible correlation with the observed trend of actual fracture porosity. Particularly noteworthy is the accuracy of the ANN predictions when the P33 parameter attained relatively high values.

To gain a more comprehensive understanding of our findings, we extended the reference depth scale for the results obtained from Well A and Well B, as depicted in Figures A3 and A4, respectively. Upon closer inspection, it became apparent that the accuracy of the ANN predictions was not entirely flawless compared to the actual values. Although the overall trend of the predicted fracture porosity closely aligned with the observed data, certain discrepancies arose, especially within the lower range of fracture porosities, and specifically, within the depth interval highlighted in a circle as 'X' (Figure A1). Within this range, the ANN tended to overestimate the fracture porosities, thereby incorrectly suggesting the presence of fractures where there are none.

This discrepancy was a primary motivation for our search for alternative machine learning algorithms, which eventually led us to adopt a hybrid ML approach. By leveraging a hybrid ML framework, we aimed to refine the accuracy of fracture porosity predictions, specifically targeting intervals where actual fracture porosity is absent but erroneously estimated by the ANN. The results of the hybrid approach are presented in the following section.

#### 4.2. Support Vector Machines-Artificial Neural Network (SVM-ANN)

In the preceding section, we established that the Artificial Neural Network (ANN) yielded higher P33 values in nonfractured layers. In order to address this issue, we adopted a two-step approach. Firstly, we employed the SVM algorithm to classify the depth interval into fractured and nonfractured layers. We utilized a radial basis kernel with the SVM algorithm to accomplish this. Following the classification, we proceeded to validate the predictions on test data. Subsequently, we exclusively utilized data from the fractured layers to predict P33 using the ANN. Our objective was to avoid overfitting the ANN model, as discussed in the previous section.

To determine the optimal configuration for our analysis, we systematically investigated the number of layers and neurons in the ANN. Through this exploration, we discovered that employing two hidden layers consisting of 10 neurons yielded the most favorable results.

We applied the ANN algorithm that utilized backpropagation with weight backtracking, similar to the previous case.

By incorporating the SVM algorithm for layer classification and carefully fine-tuning the ANN model, we aimed to enhance the accuracy of our predictions and mitigate the biases observed in nonfractured layers. This approach allowed us to overcome the challenges posed by the initial ANN predictions and made it possible to make more reliable estimations of P33 values in the fractured layers.

The SVM outcomes are presented in Table 3, which depicts the results for Wells A and B, with each comprising over two thousand data points. As shown, the SVM achieved precise predictions, allowing us to distinguish between fractured and non-fractured target formations. Well A exhibited an impressive accuracy of 96.90%, while Well B displayed a slightly lower but still commendable accuracy of 95.55%.

**Table 3.** Results of SVM for each well.

Well A: SVM algorithm predicted result		Real well logging data	
		P33 = 0	P33 > 0
Predicted well logging data	P33 = 0	1595	44
	P33 > 0	25	560
Well B: SVM algorithm predicted result		Real well logging data	
		P33 = 0	P33 > 0
Predicted well logging data	P33 = 0	1277	56
	P33 > 0	68	1383

The cross-validation on the test data for Wells A and B is presented in Figure 13. It can be seen that the R2 score and the RMSE errors were superior to those of the ANN.

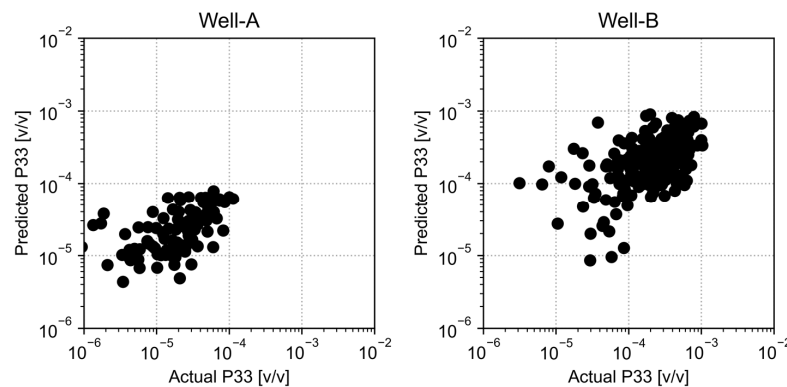


**Figure 13.** Cross plots of predicted data and the actual data used in the cross-validation using the SVM-ANN model.

As in the preceding section, the precision of the error estimates is expressed in terms of the RMSE and is tabulated in Table 4.

**Table 4.** Root Mean Square Error results for each well.

RMSE	Pure ANN	Hybrid Model
Well A	0.092	0.083
Well B	0.145	0.114

For Well A, the Pure ANN model had an RMSE of 0.092, while the Hybrid Model achieved a lower RMSE of 0.083. This suggests that the Hybrid Model outperformed the Pure ANN model in predicting values for Well A, as it had a smaller error. Similarly, the Pure ANN model had an RMSE of 0.145 for Well B, whereas the Hybrid Model achieved a lower RMSE of 0.114. In this part, the RMSE was for normalized data, in which the maximum was 1 and the minimum was 0. This was only for measuring the accuracy of the predictions.

The results are presented on different scales, specifically, 1:2000 in Figures A1 and A2, and 1:240 in Figures A3 and A4. Figures A1 and A2 illustrate that there is a similarity in the overall trend between the predicted fractural porosities and the actual fractural porosities. This means that the SVM-ANN models were able to capture the general patterns and variations in the porosity values. Figures A3 and A4 provide more detailed information. The sections highlighted with 'A' in Figures A3 and A4 indicate that the ANN underpredicted the P33 values while the SVM-ANN model tended to make more accurate porosity predictions. This suggests that the SVM-ANN model performs better than the ANN model in this respect.

However, in Figure A4, there is a layer marked with 'B', where both the ANN and SVM-ANN models failed to accurately predict the actual P33 values. This discrepancy may be attributed to the presence of overfitting in the data. Overfitting occurs when a model becomes excessively complex, fitting the noise or peculiarities of the training data rather than capturing the underlying patterns. In this study, overfitting is primarily caused by the overly complex structure of the models. To address overfitting, we adopted a strategy of simplifying the model structure when it was observed. For instance, if the ANN with three hidden layers (10, 10, 10) was found to be overfitting, we tested configurations with fewer nodes, such as (8, 8, 8), or even reduced the number of hidden layers, e.g., (10, 10). We found that in pure ANN, an optimal configuration consisted of two layers with 7 and 2 nodes, yielding relatively good results for both wells.

On the other hand, some alternative structures, such as two layers with 6 and 3 nodes, 16 and 7 nodes, or three layers with 5, 5, 5 nodes, demonstrated good results for one well but not for the other. To strike a balance between avoiding overfitting and achieving favorable outcomes for both wells, we utilized these two structures in both the pure ANN and hybrid (SVM-ANN) models. Furthermore, we observed that the surrounding zones with similar log signatures did not exhibit high degrees of fracture porosity. Consequently, the models intentionally refrained from making predictions that erroneously identified these zones as having high porosity, ensuring more accurate predictions overall.

## 5. Conclusions

In this study, we have employed an integrative approach to assess fracture porosity in a tight gas naturally fractured reservoir, i.e., the Ahnet field in Algeria. By utilizing machine learning techniques, we successfully predicted fracture porosity and conducted a comparative analysis of various methods. The results demonstrate that accurate estimations of fracture porosity can be achieved by integrating image logs and sonic scanner data. The study aimed to identify an appropriate machine learning model for fracture porosity predictions.

The findings of this analysis hold significant implications for reservoir characterization. Firstly, by utilizing basic well logs for fracture porosity estimates, we circumvent the need for acquiring expensive and time-consuming advanced well logs, which also helps mitigate the risks associated with unstable wells during logging procedures. This cost-effective approach facilitates efficient and informed decision-making during field development.

However, this study faced several limitations that should be acknowledged. Data scarcity, primarily due to confidentiality concerns expressed by the owner company, restricted the number of wells available for investigation. To enhance the robustness of the proposed methodology, future research should aim to incorporate more advanced logging data and validate the findings using core data. Additionally, the accuracy of predicted

fracture porosity outcomes was influenced by the quality of the well logs, particularly those with shallow investigation depths, as these were sensitive to the borehole conditions.

While prioritizing cost efficiency and accuracy in fracture porosity estimations, this study recognizes that neglecting expensive and time-consuming core data may limit prediction accuracy. Therefore, future research should focus on incorporating more well log and image log data to enhance fracture porosity estimations while exploring methods to minimize costs and time requirements. The SVM-ANN-based model presented in this study has proven to be a reliable tool for accurate fracture porosity estimations and could serve as a substitute in the absence of costly core datasets. Nonetheless, continuous efforts to improve the model’s performance will lead to more comprehensive and reliable fracture porosity predictions in tight gas naturally fractured reservoirs.

In summary, this research provides valuable insights into fracture porosity estimation and highlights the potential of machine learning techniques for reservoir characterization. As our understanding of these techniques deepens and data availability improves, the industry will be better equipped to optimize productions in such challenging reservoirs.

**Author Contributions:** Conceptualization, data curation, and original draft preparation, G.I. and D.I.; methodology and validation, P.P.; Validation, Investigation and Visualization, R.N.; review and editing, S.E. All authors have read and agreed to the published version of the manuscript.

**Funding:** This research received no external funding.

**Data Availability Statement:** The data presented in this study are available on request from the corresponding author. The data are not publicly available due to confidentiality by the operator.

**Conflicts of Interest:** The authors declare no conflict of interest.

### Appendix A

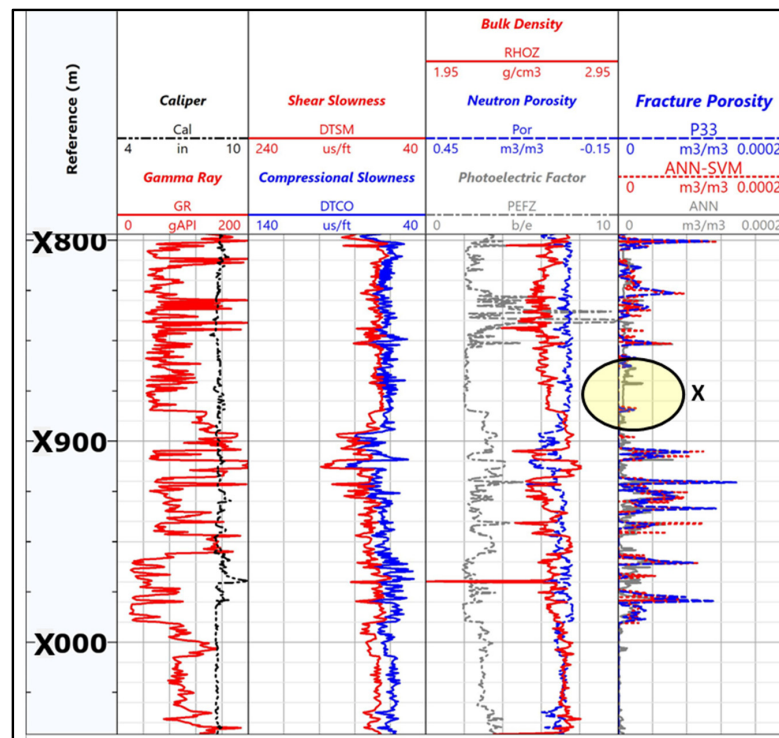


**Figure A1.** Well A presented at the depth reference scale 1:2000 m. Track I: Depth; Track II: Caliper (in black) and Gamma Ray (in red); Track III: Compressional and Shear slowness; Track IV: Neutron porosity, Bulk density and photoelectric factor; and Track V: Actual P33 porosity (in blue), ANN predicted porosity (in grey), and SVM-ANN predicted porosity (in red).

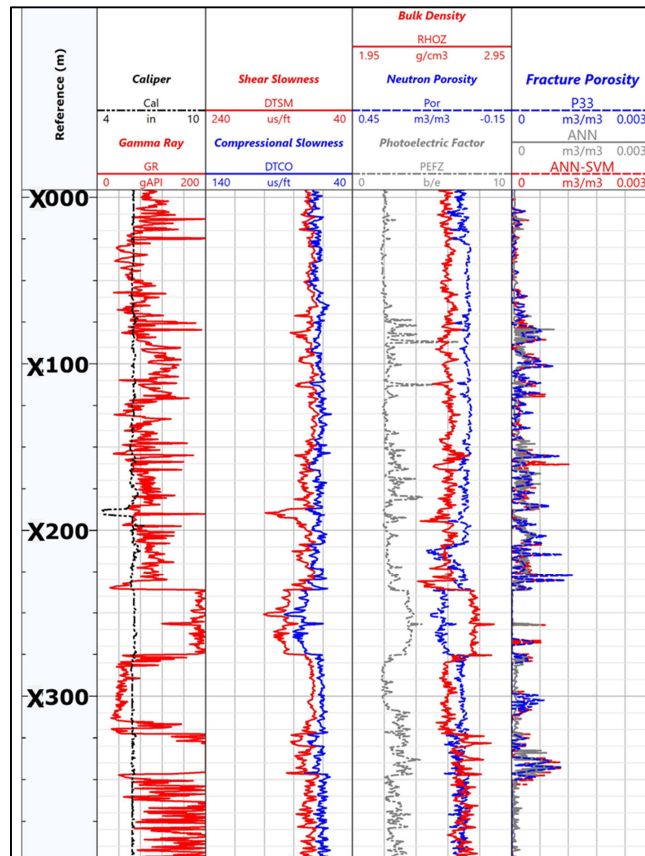


Figure A2. Well B presented at the depth reference scale 1:2000 m. Track I: Depth; Track-II: Caliper and Gamma Ray; Track III: Compressional and Shear slowness; Track IV: Neutron porosity, Bulk density, and photoelectric factor; and Track V: Actual P33 porosity (in blue), ANN predicted porosity (in grey), and SVM-ANN predicted porosity (in red).

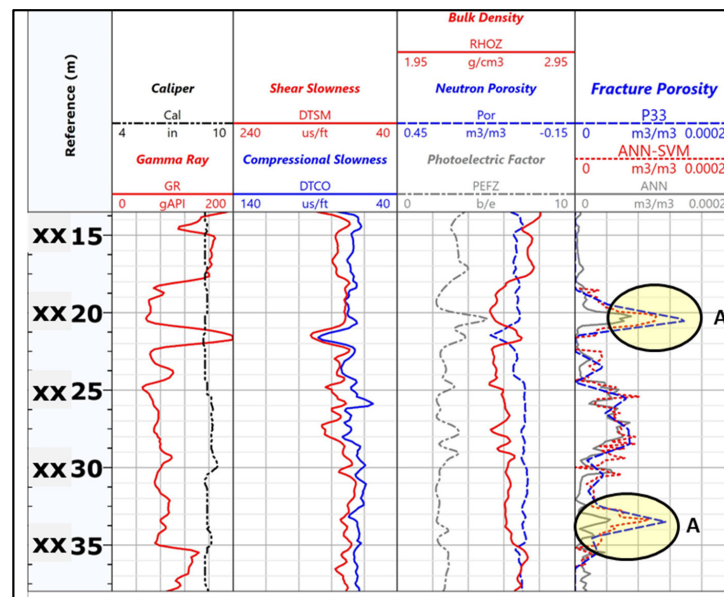
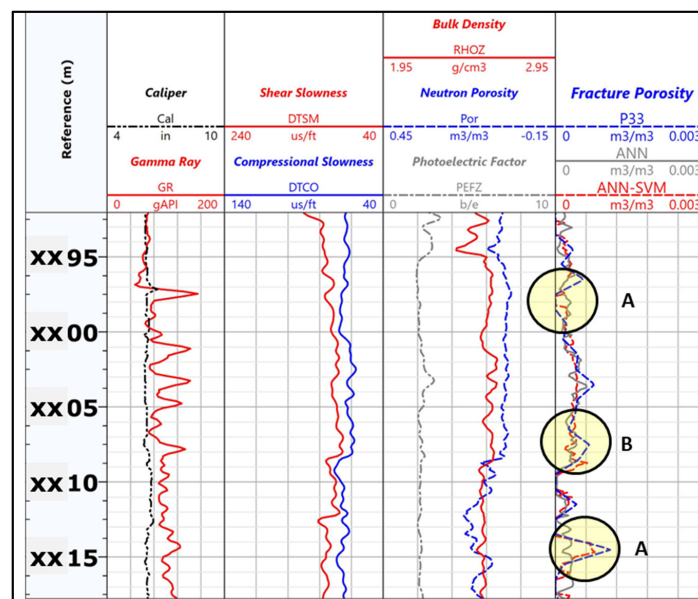


Figure A3. Well A presented at the depth reference scale 1:240 m. Track I: Depth; Track-II: Caliper and Gamma Ray; Track III: Compressional and Shear slowness; Track IV: Neutron porosity, Bulk density, and photoelectric factor; and Track V: Actual P33 porosity (in blue), ANN predicted porosity (in grey), and SVM-ANN predicted porosity (in red).



**Figure A4.** Well B presented at the depth reference scale 1:240 m: Track I: Depth; Track-II: Caliper and Gamma Ray; Track III: Compressional and Shear slowness; Track IV Neutron porosity, Bulk density, and photoelectric factor; and Track V: Actual P33 porosity (in blue), ANN predicted porosity (in grey), and SVM-ANN predicted porosity (in red).

## References

- Alagoz, E.; Wang, H.; Russell, R.T.; Sharma, M.M. New Experimental Methods to Study Proppant Embedment in Shales. In Proceedings of the 54th US Rock Mechanics/Geomechanics Symposium, Golden, CO, USA, 28 June–1 July 2020; OnePetro: Richardson, TX, USA, 2020.
- Gutmanis, J.C. Basement Reservoirs—A Review of Their Geological and Production Characteristics. In Proceedings of the IPTC 2009: International Petroleum Technology Conference, Doha, Qatar, 7–9 December 2009; European Association of Geoscientists & Engineers: Binnick, The Netherlands, 2009.
- Curtis, J.B. Fractured shale-gas systems. *Am. Assoc. Pet. Geol. Bull.* **2002**, *86*, 1921–1938. [[CrossRef](#)]
- Sulak, R. Ekofisk Field: The First 20 Years. *J. Pet. Technol.* **1991**, *43*, 1265–1271. [[CrossRef](#)]
- Alagoz, E.; Sharma, M.M. Investigating Shale-Fluid Interactions and Its Effect on Proppant Embedment Using NMR Techniques. In Proceedings of the 55th US Rock Mechanics/Geomechanics Symposium, Virtual, 18–25 June 2021; OnePetro: Richardson, TX, USA, 2021.
- Kharrat, R.; Ott, H. A Comprehensive Review of Fracture Characterization and Its Impact on Oil Production in Naturally Fractured Reservoirs. *Energies* **2023**, *16*, 3437. [[CrossRef](#)]
- Ameen, M.S.; MacPherson, K.; Al-Marhoon, M.I.; Rahim, Z. Diverse fracture properties and their impact on performance in conventional and tight-gas reservoirs, Saudi Arabia: The Unayzah, South Haradh case study. *Am. Assoc. Pet. Geol. Bull.* **2012**, *96*, 459–492. [[CrossRef](#)]
- Mahmood, M.N.; Guo, B. An Analytical Method for Optimizing Fracture Spacing in Shale Oil Reservoirs. In Proceedings of the SPE Liquids-Rich Basins Conference-North America, Odessa, TX, USA, 7–8 November 2019; OnePetro: Richardson, TX, USA, 2019.
- Laubach, S.; Marrett, R.; Olson, J. New directions in fracture characterization. *Lead. Edge* **2000**, *19*, 704–711. [[CrossRef](#)]
- Clarkson, C.; Haghshenas, B.; Ghanizadeh, A.; Qanbari, F.; Williams-Kovacs, J.; Riazi, N.; Debuhr, C.; Deglint, H. Nanopores to megafractures: Current challenges and methods for shale gas reservoir and hydraulic fracture characterization. *J. Nat. Gas Sci. Eng.* **2016**, *31*, 612–657. [[CrossRef](#)]
- Suhag, A.; Ranjith, R.; Aminzadeh, F. Comparison of Shale Oil Production Forecasting using Empirical Methods and Artificial Neural Networks. In Proceedings of the SPE Annual Technical Conference and Exhibition, San Antonio, TX, USA, 11 October 2017; SPE: Richardson, TX, USA, 2017.
- Chaki, S.; Routray, A.; Mohanty, W.K. Application of Machine Learning Algorithms for Petroleum Reservoir Characterization. In *Handbook of Petroleum Geoscience*; Wiley: Hoboken, NJ, USA, 2022; pp. 6–20. [[CrossRef](#)]
- Pothana, P.; Chatterjee, S.; Vln, A.; Deo, P.P. Prediction of Reservoir Parameters Using Support Vector Machines, A Machine Learning Approach. In Proceedings of the 5th CEWELL Symposium, Venice, Italy, 12–14 December 2020.
- Liang, B.; Liu, J.; You, J.; Jia, J.; Pan, Y.; Jeong, H. Hydrocarbon production dynamics forecasting using machine learning: A state-of-the-art review. *Fuel* **2023**, *337*, 127067. [[CrossRef](#)]

15. Shelley, R.; Oduba, O.; Melcher, H. Machine Learning and Artificial Intelligence Provides Wolfcamp Completion Design Insight. In Proceedings of the SPE/AAPG/SEG Unconventional Resources Technology Conference, Houston, TX, USA, 4 May 2021; SPE: Richardson, TX, USA, 2021.
16. Hegde, C.; Gray, K. Evaluation of coupled machine learning models for drilling optimization. *J. Nat. Gas Sci. Eng.* **2018**, *56*, 397–407. [[CrossRef](#)]
17. Choubey, S.; Karmakar, G.P. Artificial intelligence techniques and their application in oil and gas industry. *Artif. Intell. Rev.* **2021**, *54*, 3665–3683. [[CrossRef](#)]
18. Rahmanifard, H.; Plaksina, T. Application of artificial intelligence techniques in the petroleum industry: A review. *Artif. Intell. Rev.* **2019**, *52*, 2295–2318. [[CrossRef](#)]
19. Zhong, R.; Salehi, C.; Johnson, R. Machine learning for drilling applications: A review. *J. Nat. Gas Sci. Eng.* **2022**, *108*, 104807. [[CrossRef](#)]
20. Pankaj, P.; Geetan, S.; MacDonald, R.; Shukla, P.; Sharma, A.; Menasria, S.; Xue, H.; Judd, T. Application of Data Science and Machine Learning for Well Completion Optimization. In Proceedings of the Offshore Technology Conference, Houston, TX, USA, 3 May 2018; OTC: Springfield, MO, USA, 2018.
21. Misra, S.; Li, H. Noninvasive fracture characterization based on the classification of sonic wave travel times. In *Machine Learning for Subsurface Characterization*; Elsevier: Amsterdam, The Netherlands, 2020; pp. 243–287. [[CrossRef](#)]
22. Alipour, M.; Esatyana, E.; Sakhaee-Pour, A.; Sadooni, F.N.; Al-Kuwari, H.A. Characterizing fracture toughness using machine learning. *J. Pet. Sci. Eng.* **2021**, *200*, 108202. [[CrossRef](#)]
23. Zheng, Y.; Li, J.; Lin, R.; Hu, H.; Gao, K.; Huang, L.; Sciences, A.; Alamos, L. Physics-Guided Machine Learning Approach to Characterizing Small-Scale Fractures in Geothermal Fields. In Proceedings of the 46th Workshop on Geothermal Reservoir Engineering, Stanford, CA, USA, 15–17 February 2021. SGP-TR-218.
24. Singh, A.; Rabbani, A.; Regenauer-Lieb, K.; Armstrong, R.T.; Mostaghimi, P. Computer vision and unsupervised machine learning for pore-scale structural analysis of fractured porous media. *Adv. Water Resour.* **2021**, *147*, 103801. [[CrossRef](#)]
25. Rabbani, A.; Babaei, M. Image-based modeling of carbon storage in fractured organic-rich shale with deep learning acceleration. *Fuel* **2021**, *299*, 120795. [[CrossRef](#)]
26. Pandey, R.K.; Kumar, A.; Mandal, A.; Vaferi, B. Employing Deep Learning Neural Networks for Characterizing Dual-Porosity Reservoirs Based on Pressure Transient Tests. *J. Energy Resour. Technol. Trans. ASME* **2022**, *144*, 113002. [[CrossRef](#)]
27. Zazoun, R.S. Fracture density estimation from core and conventional well logs data using artificial neural networks: The Cambro-Ordovician reservoir of Mesdar oil field, Algeria. *J. Afr. Earth Sci.* **2013**, *83*, 55–73. [[CrossRef](#)]
28. Zerrouki, A.A.; Aïfa, T.; Baddari, K. Prediction of natural fracture porosity from well log data by means of fuzzy ranking and an artificial neural network in Hassi Messaoud oil field, Algeria. *J. Pet. Sci. Eng.* **2014**, *115*, 78–89. [[CrossRef](#)]
29. Bhattacharya, S.; Mishra, S. Applications of machine learning for facies and fracture prediction using Bayesian Network Theory and Random Forest: Case studies from the Appalachian basin, USA. *J. Pet. Sci. Eng.* **2018**, *170*, 1005–1017. [[CrossRef](#)]
30. Ding, Y.; Cui, M.; Zhao, F.; Shi, X.; Huang, K.; Yasin, Q. A Novel Neural Network for Seismic Anisotropy and Fracture Porosity Measurements in Carbonate Reservoirs. *Arab. J. Sci. Eng.* **2021**, *47*, 7219–7241. [[CrossRef](#)]
31. Azim, R.A. Estimation of fracture network properties from FMI and conventional well logs data using artificial neural network. *Upstream Oil Gas Technol.* **2021**, *7*, 100044. [[CrossRef](#)]
32. Boudjema, A. *Évolution Structurale du Bassin Pétrolier “Triasique” du Sahara Nord Oriental (Algérie)*; Institut Français du Pétrole: Paris, France, 1987.
33. Klitzsch, E.; Gray, C. The Structural Development of Parts of North Africa since Cambrian Time. In Proceedings of the Symposium on the geology of Libya: Tripoli, Tripoli, Lebanese, 14–18 April 1969; Faculty of Sciences, University of Libya: Benghazi, Libya, 1971; pp. 256–260.
34. Beuf, S. *Gres du Paleozoique Inferieur au Sahara*; Publications d’Institut Français du Pétrole, Collection ‘Science and Techniques du Pétrole’ No. 18; Technip: Paris, France, 1971.
35. Robertson, A.H.F.; Dixon, J.E. Introduction: Aspects of the geological evolution of the Eastern Mediterranean. *Geol. Soc. Lond. Spéc. Publ.* **1984**, *17*, 1–74. [[CrossRef](#)]
36. Guiraud, R.; Maurin, J.-C. Early Cretaceous rifts of Western and Central Africa: An overview. *Tectonophysics* **1992**, *213*, 153–168. [[CrossRef](#)]
37. Ifrene, G.E.H.; Irofti, D.; Khetib, Y.; Rasouli, V. Shear Waves Anisotropy and Image Logs Integration for Improved Fracture Characterization. In Proceedings of the 56th U.S. Rock Mechanics/Geomechanics Symposium, Santa Fe, NM, USA, 26–29 June 2022. [[CrossRef](#)]
38. Lander, L.A.; Silva, A.; Chiquito, J.; Cadena, A. Improved Fracture Characterization in the La Paz Field: A Case Study. In Proceedings of the SPE Latin American and Caribbean Petroleum Engineering Conference, Quito, Ecuador, 18 November 2015; OnePetro: Richardson, TX, USA, 2015.
39. Maeso, C.; Dubourg, I.; Quesada, D.; ElNour, W.A. Uncertainties in Fracture Apertures Calculated from Electrical Borehole Images. In Proceedings of the International Petroleum Technology Conference, Riyadh, Saudi Arabia, 21–23 February 2022; OnePetro: Richardson, TX, USA, 2015. [[CrossRef](#)]
40. Li, H. *Statistical Learning Methods*; Tsinghua Univ. Press: Beijing, China, 2012; pp. 95–115.

41. Huang, Z.; Shimeld, J.; Williamson, M.; Katsube, J. Permeability prediction with artificial neural network modeling in the Venture gas field, offshore eastern Canada. *Geophysics* **1996**, *61*, 422–436. [[CrossRef](#)]
42. Tariq, Z.; Elkatatny, S.M.; Mahmoud, M.A.; Abdulraheem, A.; Abdelwahab, A.Z.; Woldeamanuel, M. Estimation of Rock Mechanical Parameters Using Artificial Intelligence Tools. In Proceedings of the 51st US Rock Mechanics/Geomechanics Symposium, San Francisco, CA, USA, 25–28 June 2017; OnePetro: Richardson, TX, USA, 2017.
43. Agatonovic-Kustrin, S.; Beresford, R. Basic Concepts of Artificial Neural Network (ANN) Modeling and Its Application in Pharmaceutical Research. *J. Pharm. Biomed. Anal.* **2000**, *22*, 717–727. [[CrossRef](#)]
44. Ebrahimi, A.; Izadpanahi, A.; Ebrahimi, P.; Ranjbar, A. Estimation of shear wave velocity in an Iranian oil reservoir using machine learning methods. *J. Pet. Sci. Eng.* **2022**, *209*, 109841. [[CrossRef](#)]
45. Wang, P.; Peng, S. On a new method of estimating shear wave velocity from conventional well logs. *J. Pet. Sci. Eng.* **2019**, *180*, 105–123. [[CrossRef](#)]
46. Suthaharan, S.; Suthaharan, S. *Machine Learning Models and Algorithms for Big Data Classification: Thinking with Examples for Effective Learning*; Springer: Berlin/Heidelberg, Germany, 2016; pp. 207–235.
47. Ying, X. An Overview of Overfitting and its Solutions. *J. Phys. Conf. Ser.* **2019**, *1168*, 022022. [[CrossRef](#)]

**Disclaimer/Publisher’s Note:** The statements, opinions and data contained in all publications are solely those of the individual author(s) and contributor(s) and not of MDPI and/or the editor(s). MDPI and/or the editor(s) disclaim responsibility for any injury to people or property resulting from any ideas, methods, instructions or products referred to in the content.